ChemSusChem

Research Article
doi.org/10.1002/cssc.202200194

Chemistry Europe
European Chemical Societies Publishing

www.chemsuschem.org

Selective Conversion of HMF into 3-Hydroxymethylcyclopentylamine through a One-Pot Cascade Process in Aqueous Phase over Bimetallic NiCo Nanoparticles as Catalyst

Beatriz Hurtado,[a] Karen S. Arias,[a] Maria J. Climent,*[a] Patricia Concepción,[a] Avelino Corma,*[a] and Sara Iborra*[a]

5-hydroxymethylfurfural (HMF) has been successfully valorized into 3-hydroxymethylcyclopentylamine through a one-pot cascade process in aqueous phase by coupling the hydrogenative ring-rearrangement of HMF into 3-hydroxymethylcyclopentanone (HCPN) with a subsequent reductive amination with ammonia. Mono- (Ni@C, Co@C) and bimetallic (NiCo@C) nanoparticles with different Ni/Co ratios partially covered by a thin carbon layer were prepared and characterized. Results showed that a NiCo catalyst, (molar ratio Ni/Co = 1, $Ni_{0.5}Co_{0.5}$@C), displayed excellent performance in the hydrogenative ring-rearrangement of HMF into HCPN (> 90% yield). The high selectivity of the catalyst was attributed to the formation of NiCo alloy structures as hydrogenating sites that limited competitive reactions such as the hydrogenation of furan ring and the over-reduction of the formed HPCN. The subsequent reductive amination of HPCN with aqueous ammonia was performed giving the target cyclopentylaminoalcohol in 97% yield. Moreover, the catalyst exhibited high stability maintaining its activity and selectivity for repeated reaction cycles.

Introduction

The production of chemicals from renewable biomass is paving the way for a decarbonization program. An approach for producing chemicals from biomass is through the transformation of the biomass-derived platform molecules.[1–3] Among them, 5-hydroxymethylfurfural (HMF), produced by the acid-catalyzed dehydration of hexoses, represents one of the most promising biobased platform molecules for the production of fine chemicals due to its multifunctional structure. HMF contains an aldehyde group, a hydroxymethyl group, and furan ring functions that can undergo a variety of chemical reactions, such as hydrogenation, oxidation, esterification, etherification, hydrogenolysis, ring-opening, and others, leading to a wide variety of high value-added chemicals.[4–7] In the last years, our group has devoted an important effort to the molecular design of catalysts[8] for production of chemicals and, more specifically, to valorize HMF into different value-added molecules such as drug precursors, surfactants, and monomers.[9–12] Recently, the hydrogenative ring-rearrangement of HMF into 3-hydroxymethylcyclopentanone (HCPN) has attracted increasing attention as a valuable intermediate for manufacturing a variety of pharmaceuticals, polymers, flavours, and so on.[13–15] Here we present the valorization of HMF into 3-hydroxymethylcyclopentylamine through a new one-pot cascade process using non-noble metals as hydrogenating catalysts. Cyclopentylamine derivatives are valuable chemicals used as starting compounds for the synthesis of a variety of fine chemicals,[16] and particularly 3-hydroxymethylcyclopentylamine has been used as ribose motif for the preparation of carbocyclic nucleosides analogues with a diversity of important biological activities such as antiviral and antineoplastic activities.[17] Moreover, our prospective studies considered that this compound could be of interest as biobased monomer while the aminoalcohol functionalities provide high versatility to produce biobased surfactants, such as ammonium salts or betaines.

The hydrogenative ring-rearrangement of HMF into HCPN occurs when HMF is hydrogenated at elevated temperatures (usually higher than 140 °C) in aqueous media. In fact, it has been shown that this transformation does not take place when other solvents such as THF, ethanol, 1,4-dioxane, isopropanol, or THFA (Tetrahydrofurfuryl alcohol) are used.[18]

The reaction mechanism is not completely clarified, but the most accepted reaction route involves as a first step the hydrogenation of the formyl group of HMF into 2,5-bis(hydroxymethyl)furan (BHMF). Then, a Piancatelli ring-rearrangement of BHMF promoted by acid sites and water affords

[a] Dr. B. Hurtado, Dr. K. S. Arias, Prof. M. J. Climent, Dr. P. Concepción, Prof. A. Corma, Prof. S. Iborra
Instituto de Tecnología Química (UPV-CSIC)
Universitat Politècnica de València
Avda dels Tarongers s/n, 46022,
Valencia (Spain)
E-mail: mjcliol@qim.upv.es
acorma@itq.upv.es
siborra@itq.upv.es

Supporting information for this article is available on the WWW under https://doi.org/10.1002/cssc.202200194

This publication is part of a collection of invited contributions focusing on "Green Conversion of HMF". Please visit chemsuschem.org/collections to view all contributions.

4-hydroxy-4-hydroxymethyl-2-cyclopentenone. Further deoxygenation (dehydration and/or hydrogenolysis) and hydrogenation reactions result in HCPN (Scheme 1). In addition, 1-hydroxy-2,5-hexanedione (HHD) can be also formed, which by intramolecular aldol condensation and subsequent hydrogenation yields 3-hydroxymethylcyclopentanone (HCPN).[13,18,19] However, two side reactions that reduce the selectivity to HCPN are the hydrogenation of the furan ring giving 2,5-bis(hydroxymethyl)tetrahydrofuran (BHMTHF), which is unable to undergo rearrangement as a result of the difficulty in opening saturated furan rings,[20] and the further hydrogenation of HCPN into 3-hydroxymethylcyclopentanol (HCPO).

The hydrogenative ring-rearrangement of HMF in water has been mainly performed using noble metal catalysts. Ohyama et al. firstly reported the hydrogenative ring-rearrangement of HMF using Au/Nb_2O_5, at 140 °C and 80 MPa H_2 achieving 86% yield of HCPN.[13] Later, a variety of noble metals (Pt, Pd, Ir, Au) loaded on supports such as acidic metal oxides or metal-organic frameworks[19,21–24] has been reported to perform the reaction with different success. In Table S1 some representative results for the production of HCPN with noble metal catalysts are summarized. However, the cost and scarcity of noble metals have promoted an increasing interest for low-cost non-noble metals catalysts that can still give good conversions and selectivity[25] as a promising strategy for a more sustainable chemistry. Nevertheless, to date, studies of the hydrogenative ring-rearrangement of HMF for the production of cyclopentanone derivatives using non-noble metal-based catalysts are scarce, and most of them are based on Ni catalysts. For instance, Perret et al. reported that the hydrogenation of HMF in water over Ni on Al_2O_3, prepared from Ni–Al layered double hydroxides, gave 81% HCPN yield at 140 °C and 2 MPa H_2 after 6 h, with BHMTHF (8%) and HHD (11%) as the other detected products. However, at 80 °C, the hydrogenation of the furan ring into BHMTHF was the main process.[26] Later, the same authors reported the hydrogenation of HMF in water over Cu and Co on Al_2O_3, prepared from the corresponding layered double hydroxides. Using Cu/Al_2O_3 as catalyst and working at 140 °C and 2 MPa a total conversion of HMF was achieved after 6 h, with 79% selectivity to HCPN. BHMF, 4-hydroxymethyl-2-cyclopentenone (HCPENT), and HHD were also detected in low amounts (5–7%). However, with Co/Al_2O_3 the main product was HCPO (61% yield), which was formed by further hydrogenation of the cyclopentanone derivative.[27] More recently, Morales et al.[28] prepared Ni catalysts on different carbon supports that were tested in the hydrogenation of HMF in water. The authors found that carbon supports limit to some extent the reactivity of Ni towards hydrogenation of the furan ring. When the reaction was performed with an optimized catalyst (Ni on commercial high-surface-area graphite) under 30 bar H_2 pressure, at 180 °C, 100% HMF conversion was achieved in 3 h with 87% selectivity to HCPN, while BHMTHF was not detected. Moreover, the authors proved that the rearrangement of the furan ring of HMF does not require the presence of an acidic support. Additionally, the catalyst was active for the hydrogenation of HMF into BHMF when working at 60 °C.

Bimetallic catalysts have been recognized as an interesting strategy to increase the performance of metal-based catalysts. In fact, for the valorization of highly functionalized and reactive biomass derived furans, bimetallic catalysts are of interest for enhancing activity and tuning selectivity towards the desired product.[29] Xu and co-workers[18] have studied the hydrogenative ring-rearrangement of HMF over different bimetallic Ni-based catalysts prepared by the pyrolysis of MOF precursors. While the monometallic Ni/C catalyst gave BHMTHF (complete hydrogenation of HMF) as the only product, the bimetallic NiCu/C, NiFe/C, and NiCo/C gave HCPN; the NiCu/C catalyst was the most selective to HCPN (50% HCPN yield at 94% HMF conversion). Isotope experiments in $H_2{}^{18}O_2$ showed that water acts not only as a solvent and reactant but also as a source of protons that creates the acidic conditions to promote the ring-rearrangement. Recently, Li et al.[30] showed that $Ni–Fe/\gamma Al_2O_3$ (with an optimized Ni/Fe ratio) exhibited increased selectivity to HCPN compared with monometallic catalysts, demonstrating the synergistic effect of the NiFe alloy and achieving complete conversion of HMF with 86% selectivity to HCPN at 160 °C under 4 MPa H_2 for 4 h. Despite these promising results, the main problem associated with supported non-noble metal

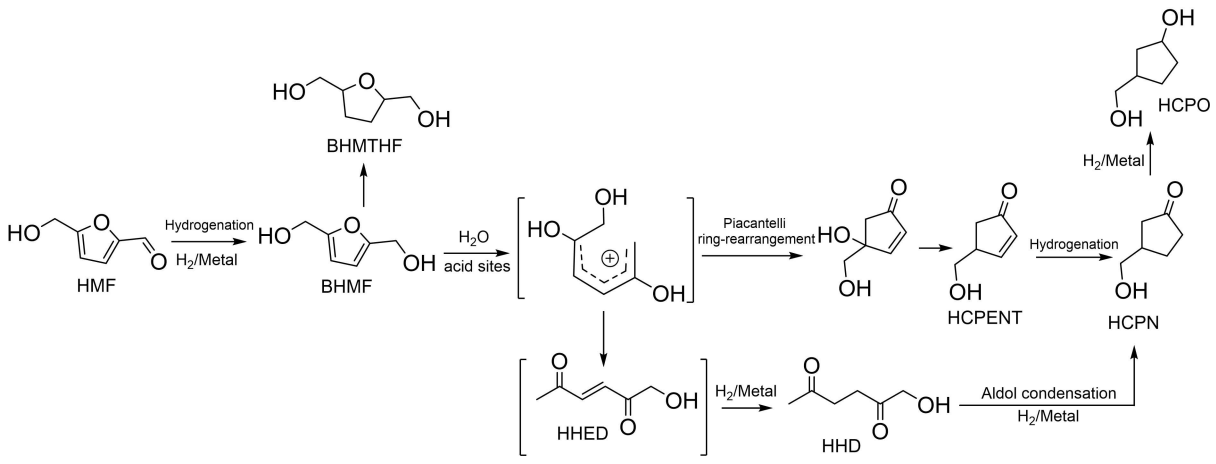

Scheme 1. Proposed reaction pathways for the hydrogenative ring-opening of HMF according to literature.[18,19]

nanoparticles is catalyst deactivation. It is mainly associated with metal agglomeration, metal oxidation, and leaching, or even hydration of the support under the reaction conditions, which limit catalyst recyclability. It is then of interest to develop non-noble metal catalysts able to perform efficiently in aqueous phase at relatively high temperatures.

In previous studies, our group has developed mono- and bimetallic catalysts based on non-noble metal nanoparticles (Co@C, CoNi@C, CoW@C, FeCu@C) partially covered by a few layers of carbon. Exposition to air during handling of the catalysts generates surface metal oxide patches together with still reduced metal. Then, the oxide is more easily reduced Cby the hydrogen dissociated on the metal part of the catalyst. The carbon layers present cracks that allow diffusion of the reactants to the metal. In addition, the carbon coating promotes the in-situ reduction of oxide species on the surface of the metal nanoparticle under reaction conditions, while protecting the non-noble metal from agglomeration, over-oxidation, and metal leaching.[12,31–33] These catalysts showed excellent activity and selectivity for the chemoselective reduction of nitroarenes into anilines, reduction of levulinic acid into γ-valerolactone,[32,33] hydrogenation of quinolines,[31] as well as for the selective reduction of HMF to BHMF.[12]

Considering the high stability and good performance of these nanoparticles in hydrogenation reactions, as well their simple and green preparation method, we thought to adapt the catalysts for the hydrogenative ring-rearrangement of HMF. Thus, we have prepared mono- (Ni, and Co) and bimetallic Ni based catalysts (NiCo) to perform the hydrogenative ring-rearrangement of HMF in water. We will show that by controlling the Ni/Co molar ratio it is possible to achieve high conversion and selectivity to HPCN. Moreover, we have coupled, for the first time, the hydrogenative ring-rearrangement of HMF into HCPN with the reductive amination of HCPN with aqueous ammonia to produce the corresponding cyclopentylaminoalcohol, that is, 3-hydroxymethylcyclopentylamine in a one-pot cascade process (Scheme 2).

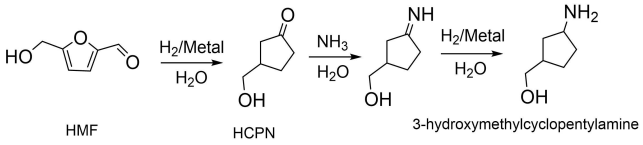

Scheme 2. Cascade process to produce 3-hydroxymethylcyclopentylamine from HMF.

Results and Discussion

Catalyst preparation and characterization

According to previous works,[32,34] non-noble metal nanoparticles covered by thin carbon layers were prepared using metal oxide nanoparticles by a precipitation-calcination procedure. After coating using glucose as carbon precursors, the M-$(OH)_x$@glucose nanocomposites were obtained by a hydrothermal process. The subsequent treatment in N_2 at 600 °C led to the graphitization of carbon and the reduction of oxides into metallic nanoparticles, which are partially covered by carbon. Thermogravimetric (TG) analysis of the catalysts and elemental analysis showed that the amount of C in the catalysts was around 5 %, which agrees with the amount of carbon estimated based on the thickness of the carbon coatings, determined by transmission electron microscopy (TEM; 5–6 wt %).

X-ray diffraction (XRD) patterns of monometallic (Co@C, Ni@C) and bimetallic ($Ni_{0.25}Co_{0.75}$@C, $Ni_{0.5}$ $Co_{0.5}$@C, $Ni_{0.75}Co_{0.25}$@C) nanoparticles (NPs) are presented in Figure 1. Diffraction peaks at 44.5, 51.8, and 76.3° corresponding to Ni^0 (44.5), (51.8), and (76.3) (PDF 00-004-0850)[35] are observed in the Ni@C sample (Figure 1, green line), while in the Co@C sample, the peaks appears at 44.3, 51.5, and 75.8°, assigned to Co^0 (44.2), (51.5), and (75.8) (PDF 00-015-0806) (Figure 1, black line). In the bimetallic NPs, the XRD peaks are located between those of Ni^0 and Co^0. These shifts of the XRD peak positions have been attributed in several studies to the alloying effect of Ni and Co,[35–41] and in our case the shift to lower angles can be associated to a gradual replacement of Ni with Co atoms at increasing cobalt content in the NiCo@C samples. Variation of the lattice parameter of the alloy phase with the Co content follows Vegard's law[42] (linear correlation coefficient *R* of

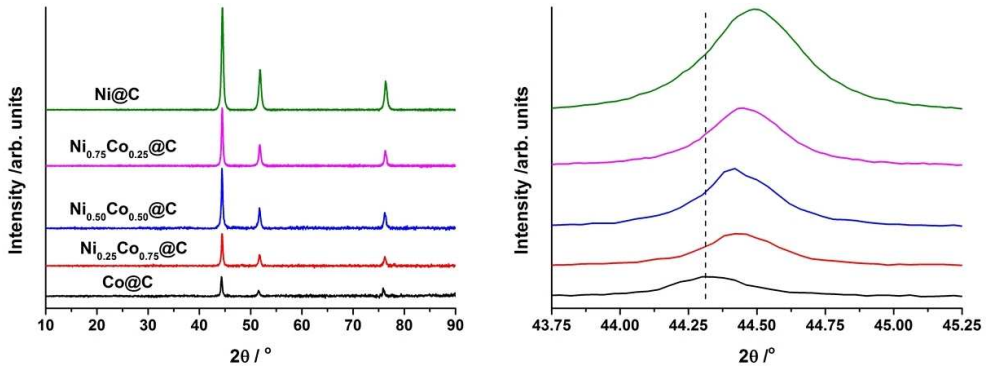

Figure 1. XRD patterns of Co@C, Ni@C, and NiCo@C bimetallic nanoparticles with different chemical compositions. Inset showing the enlarged view of (111) peak, which is slightly shifted to a higher angle with increasing Ni content.

0.9984) as shown in Figure S1, indicating the formation of a solid solution between Ni and Co.

The morphology, atom distribution, and particle size of monometallic and bimetallic nanoparticles prepared starting from different molar ratios of metal salt precursors were characterized by high-resolution (HR)TEM and energy-dispersive X-ray spectroscopy (EDS) elemental mapping. HRTEM images (Figure 2a–f; see also Figure S2) show that the non-noble metal nanoparticles range from 10 to 100 nm. Furthermore, HRTEM images of mono and bimetallic samples show a highly integrated nanostructure of layered carbon-coated metal nanoparticles (Figures 2 and S2). The lattice spacing of monometallic Co@C and Ni@C catalysts is 0.20 nm (Figure 2b,f, respectively), which is attributed to the (111) plane of metallic cobalt and nickel species. Moreover, some Co_3O_4 patches can also be found in the Co@C NPs, while NiO is observed in the Ni@C NPs, which should come from re-oxidation of the surface of metallic NPs after preparation and exposure to air (see Figure 2b,f).[31,32]

On the other hand, HRTEM images of $Ni_{0.5}Co_{0.5}$@C sample (Figure 2d) show a lattice spacing of 0.21 nm, which corresponds to the interplanar space between (111) facet of Ni–Co.[43] The interplanar space of 0.21 nm was also found in samples $Ni_{0.75}Co_{0.25}$@C and $Ni_{0.25}Co_{0.75}$@C (Figures S2), indicating that alloyed species are also formed on these samples.

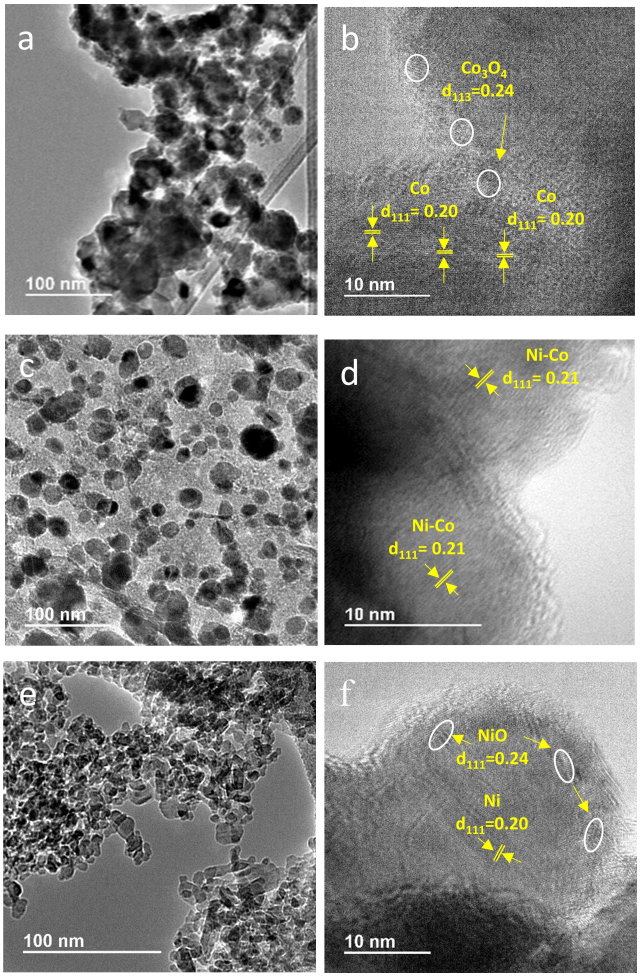

Figure 2. HRTEM images of catalyst (a,b) Co@C NPs, (c,d) $Ni_{0.5}Co_{0.5}$@C NPs, and (e,f) Ni@C NPs.

High-angle annular dark-field scanning transmission electron microscopy (HAADF-STEM) images and the corresponding EDS elemental mapping of Co and Ni of bimetallic NiCo samples are presented in Figure 3. As can be seen, spatial distributions for Co, Ni, and C overlap very well with each other, in agreement with the formation of NiCo alloyed structures.

The X-ray photoelectron spectroscopy (XPS) spectra of mono- and bimetallic samples are shown in Figure S3, and their binding energy (BE) and surface chemical composition are summarized in Table 1. In all samples, both metallic and oxidized species are present. In the pure Co@C and Ni@C samples, oxidized species predominate over metallic cobalt or nickel. In fact, the Auger parameter of Cobalt [α(Co)] in the Co@C sample corresponds to Co_3O_4, and in the Ni@C sample, the nickel Auger parameter [α(Ni)] corresponds to NiO. This is in agreement with the HRTEM analysis, where both oxides are observed (Figure 2b,f). In contrast to the monometallic samples, the amount of oxidized species decreases when bimetallic samples are considered. The surface exposed metallic component in the cobalt part increases when increasing the cobalt fraction in the bimetallic samples (i.e., going from 0.2% in $Ni_{0.75}Co_{0.25}$@C to 7.2% in $Ni_{0.50}Co_{0.50}$@C and finally 11.7% in $Ni_{0.25}Co_{0.75}$@C), while the nickel metallic part remains constant around 5% in all samples. The characterization results show surface Co^0/Ni^0 for the NiCo@C catalysts being 0.04, 1.5, and 2.1 in the $Ni_{0.75}Co_{0.25}$@C, $Ni_{0.50}Co_{0.50}$@C, and $Ni_{0.25}Co_{0.75}$@C samples, respectively. Regarding the BE of cobalt and nickel, the Co $2p_{3/2}$ core level shows several components located at 778.2 ± 0.2 eV for Co^0, 779.2 ± 0.6 eV for Co^{3+}, and 781.8–780.5 eV together with two shake-up peaks at higher BE (783.0–787.2 eV) characteristic of Co^{2+}.[28,44–46] The BE of all the components are shifted to lower values in the bimetallic samples with respect to the monometallic ones, being 0.2 eV for Co^0 and 0.4–1.3 eV for the cobalt oxide. Similar shifts in the Co^0 BE have been attributed to the formation of NiCo alloys.[35,38] The shift in the oxide component is more complicated to assign due to the different surface oxidation degrees of the sample. Regarding to the Ni $2p_{3/2}$ core level the component at 852.0 ± 0.6 eV is ascribed to Ni^0, and the 853.3–856 eV peaks together with satellite peaks at higher BE (858.1–863.1 eV) are characteristic of Ni^{2+}. In this case a higher BE shift (+0.6 eV) is observed in the bimetallic samples compared to the monometallic, where the Ni $2p_{3/2}$ BE of 852.6 eV of the bimetallic compounds has been attributed by Li and co-workers to NiCo alloy.[38] From these results, we can conclude that NiCo alloyed species are present in the bimetallic samples, in good agreement with HRTEM data where the lattice parameters characteristic of NiCo alloy are observed. However, based on the above-mentioned surface Co^0/Ni^0 ratio, the coexistence of segregated metallic phases can also be assumed. Thus, a Co^0/Ni^0 value of 0.2 (as in the $Ni_{0.75}Co_{0.25}$@C sample) indicates the coexistence of segregated Ni^0, while the value of 2.1 (as in the $Ni_{0.25}Co_{0.75}$@C samples) corresponds to segregated Co^0. In parallel to this, the formation of a higher extension of alloyed NiCo species can be retrieved from the Auger parameter, which gives additional insight in the electronic state of

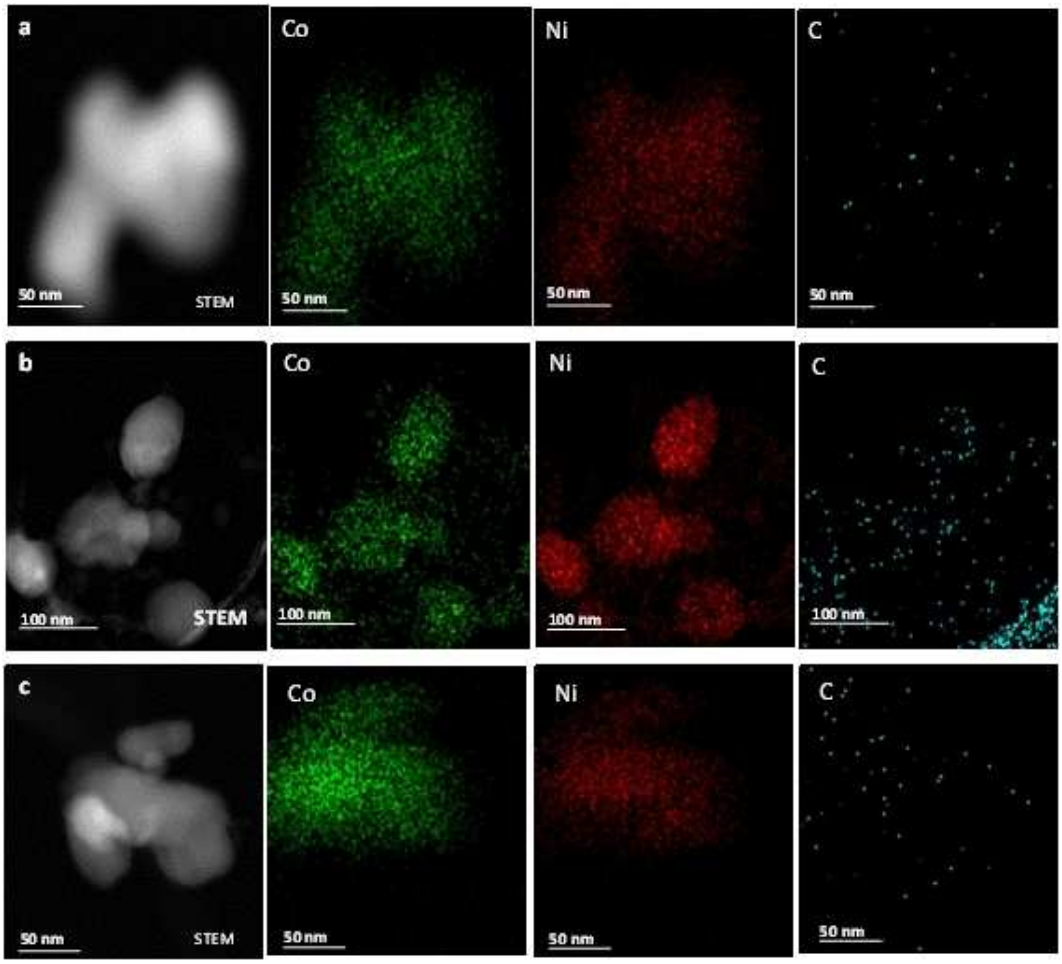

Figure 3. HAADF-STEM images of the bimetallic catalysts and elemental mapping of C, Co, and Ni. (a) $Ni_{0.5}Co_{0.5}$@C, (b) $Ni_{0.75}Co_{0.25}$@C, and (c) $Ni_{0.25}Co_{0.75}$@C.

transition metal compounds.[47] In particular, in both $Ni_{0.50}Co_{0.50}$@C and $Ni_{0.25}Co_{0.75}$@C samples, the nickel Auger parameter differs from Ni^0 (1699 eV), while is analogous to AlNi and $Al_{70}Co_{15}Ni_{15}$ alloys (1698.0 eV),[48] and in the $Ni_{0.75}Co_{0.25}$@C t is 1701.9 eV close to NiO, in agreement with the higher fraction of oxidized species in the latter sample.

Hydrogenative ring-rearrangement of HMF into HCPN

Catalytic hydrogenation and ring-rearrangement of HMF to HCPN in aqueous medium was studied using mono (Ni@C and Co@C) and bimetallic NiCo@C nanoparticles with different Ni/Co ratios at 140 °C and 20 bar H_2 pressure. Catalysts were previously reduced according temperature-programmed reduction (TPR) measurements (Figure S4). When the reaction was performed using Ni@C catalysts, HMF was first hydrogenated at low reaction rate into BHMF that subsequently underwent ring-rearrangement to HCPN. Different intermediates that disappear with time in favor of HCPN, such as HHD and HCPENT, were also detected (see Figure 4 and Table 2), indicating that HMF follows same reaction route as the previously observed one

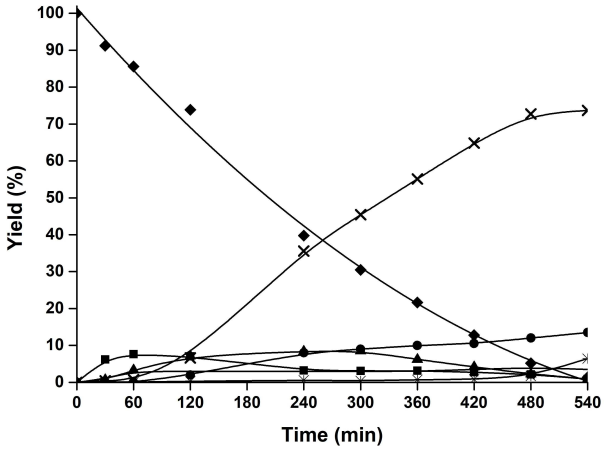

Figure 4. Kinetics of the hydrogenative ring-rearrangement of HMF using Ni@C catalyst. Reaction conditions: HMF (0.5 mmol), Ni@C (20 mg), H_2O (5 mL), 140 °C, and 20 bar of H_2. HMF (◆), BHMF (▪), HCPENT (▲), HCPN (×), HCPO (✱), BHMTHF (●).

using noble and non-noble metal-based catalysts. Moreover, the competitive hydrogenation of the furan ring giving

Table 1. XPS BE values and surface composition for the monometallic and bimetallic catalysts.

Sample	Co $2p_{3/2}$ BE[a] [eV]			Ni $2p_{3/2}$ BE[a] [eV]			Co/Ni/C/O	Co/Ni	Co^0/Co^{n+} Ni^0/Ni^{n+}	α(Co)[b] α(Ni)[c]
	Co^0	Co^{3+}	Co^{2+}	Ni^0	Ni^{2+}	N+2				
Co@C	778.4 (5.2%)	779.8 (5.6%)	781.8 (11.2%) 783.9 (sat) (3.4%) 787.2 (sat) (7.4%)	–	–	–	32.4:–:15.6:1.9	–	5.2:7.6 –:–	1554.4 Co_3O_4
Ni@C	–	–	–	852.0 (1.3%)	853.3 (0.9%)	855.6 (10.8%) 858.6 (sat) (6.7%) 863.1 (sat) (3.6%)	–:23.6:24.8:51.9	–	–:– 1.3:22	1701.2 NiO
$Ni_{0.75}Co_{0.25}$@C	778.2 (0.2%)	779.2 (2.4%)	781.4 (2.8%) 783.7 (sat) (1.4%) 786.9 (sat) (1.4%)	852.6 (5.0%)	854.0 (0.9%)	855.9 (7.6%) 861.3 (sat) (4.0%)	8.3:17.5:22.7:51.5	1:2	0.2:8 5:12.5	1554.5 Co_3O_4 1701.9 NiO
$Ni_{0.50}Co_{0.50}$@C	778.2 (7.2%)	–	780.8 (5.4%) 783.2 (sat) (2.7%) 786.5 (sat) (1.5%)	852.7 (4.6%)	854.0 (0.1%)	856.1 (1.9%) 860.1 (sat) (0.8%)	16.7:7.4:26.6:49.5	1:0.5	7.2:9.6 4.6:2.8	1552.1 Co^0 1698.3 NiCo
$Ni_{0.25}Co_{0.75}$@C	778.2 (11.7%)	–	780.5 (4.4%) 783.0 (sat) (2.5%) 785.6 (sat) (0.8%)	852.7 (5.8%)	–	856.1 (0.4%) 859.0 (sat) (0.9%)	19.1:6.9:17.1:6.8	2.7:1	11.7:7.7 5.8:1.3	1552.1 Co^0 1698.3 NiCo

[a] Surface composition given in parentheses (Sat = Satellite peak).[b] α(Co) Auger parameter of cobalt calculated as BE(Co $2p_{3/2}$) + KE(CoL3VV). [c] α(Ni) Auger parameter of nickel calculated as BE(Ni $2p_{3/2}$) + KE(NiL3VV). Kinetic Energy associated to the Auger peak.

Table 2. Results of the hydrogenative ring-rearrangement of HMF over bimetallic and monometallic catalysts.[a]

Entry	Catalyst	r_o[b] [mmol $min^{-1} \times 10^{-3}$]	t [h]	Conv. [%]	Yield [%] BHMF	BHMTHF	HHD	HCPENT	HCPN	HCPO	Sel. [%] HCPN	HCPO
1	Ni@C	1.48	9	99	1	16	3	2	74	6	77	2
2	$Ni_{0.75}Co_{0.25}$@C	1.75	9	99	2	10	3	2	79	3	80	3
3	$Ni_{0.5}Co_{0.5}$@C	2.38	7	99	2	<1	0	2	92	2	94	2
4	$Ni_{0.25}Co_{0.75}$@C	3.64	5	99	3	<1	9	2	63	22	64	22
5	Co@C	6.53	4	99	1	<1	2	<1	41	54	41	54
6	Co@C + Ni@C	4.80	4.5	100	<1	7	2	<1	65	25	65	25

[a] Reaction conditions: 0.5 mmol of HMF, 20 mg of catalyst, 5 mL H_2O as solvent, 140 °C, and 20 bar H_2. [b] Initial reaction rate of disappearance of HMF calculated when the conversion of HMF is below 20%.

BHMTHF, which is stable and does not suffer ring opening, was also observed. This result agrees with the strong ability of Ni-based catalysts for C=C hydrogenation that promotes the hydrogenation of the furan ring.[26,37,49] Thus, the flat adsorption mode of HMF over Ni promotes the activation of both the carbonyl group and the furan ring.[50] As can be observed in Table 2, at complete conversion of HMF (9 h reaction time), 74% yield of HPCN and 16% of BHMTHF were achieved. Moreover, a 6% yield of HCPO, the cyclopentanol derivative coming from the further hydrogenation of the carbonyl group of HPCN, was also detected. Additionally, blank experiments performed in absence of catalyst or in the absence of hydrogen showed that the reaction practically did not occur.

Considering that the introduction of a secondary metal can alter the catalytic activity of the Ni catalyst,[18] we prepared different NiCo@C samples with different Ni/Co ratios that were tested for the hydrogenative ring-rearrangement of HMF. Results presented in Table 2 show that when the amount of Co incorporated in the Ni samples increases from 25 to 50% (entries 2 and 3, and Figure 5 and S5, respectively) the initial reaction rate of disappearance of HMF increases, while the hydrogenation of the furan ring into BHMTHF is drastically reduced (from 16% for Ni@C to <1% for $Ni_{0.5}Co_{0.5}$@C). Accordingly, the selectivity to HPCN increases with the Co content, and particularly for the $Ni_{0.5}Co_{0.5}$@C sample, the selectivity to HPCN was the highest (94%), while other intermediate products (BHMF and HCPENT) were detected in very low amounts (see entry 3, Table 2). Moreover, the activity of these samples for hydrogenating HPCN into HCPO is low, and HCPO is detected in very low concentration (2–3%).

Further increase in the Co content (Table 2, entry 4, and Figure S6), increases the reaction rate of disappearance of HMF but decreases considerably the selectivity to HCPN in favor of the cyclopentanol derivative (HCPO), while the monometallic

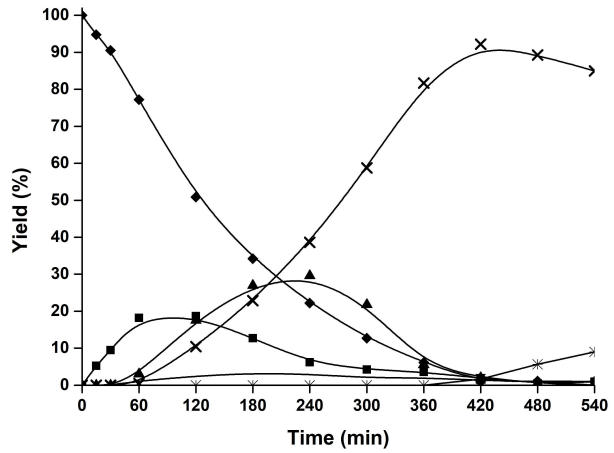

Figure 5. Kinetics of the hydrogenative ring-rearrangement of HMF using $Ni_{0.5}Co_{0.5}$@C catalyst. Reaction conditions: HMF (0.5 mmol), $Ni_{0.5}Co_{0.5}$@C (20 mg), H_2O (5 mL), 140 °C, and 20 bar of H_2. HMF (◆), BHMF (▪), HCPENT (▲), HCPN (×), HCPO (✱), HHD (—).

Co@C is more selective towards HCPO than to HCPN (entry 5 and Figure 6). This behavior should be associated with the superior interaction of the Co with the ketone carbonyl group[51] and agrees with the previously reported results on hydrogenative ring-opening of HMF with Co/Al_2O_3[52] where the main product obtained was HCPO. In fact, in our case 95% yield to HCPO can be achieved within 8 h reaction time with Co@C catalyst (see Figure 6). Additionally, other by-products such as linear alcohols or compounds derived from C—O hydrogenolysis (3-methylcyclopentanol and 5-methyl-2-furylmethanol) or C—C bond cleavage (cyclopentanone and furfuryl alcohol) were not detected with the different catalysts tested.

Considering the XPS and HRTEM results of the different catalysts it appears that the introduction of Co in the Ni samples generates the formation of NiCo alloyed structures that have an impact on selectivity to HPCN. This is particularly

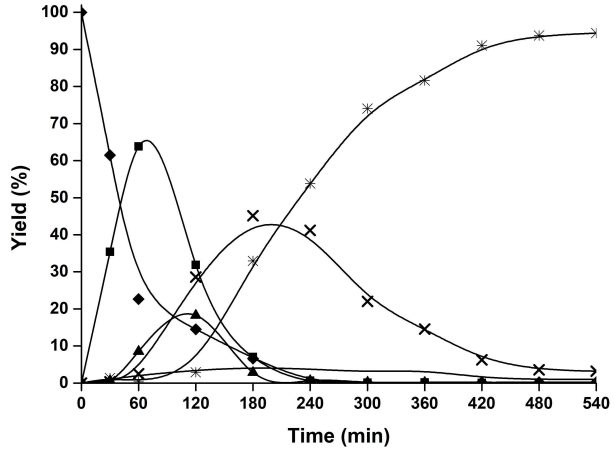

Figure 6. Kinetics of the hydrogenative ring-rearrangement of HMF using Co@C catalyst. Reaction conditions: HMF (0.5 mmol), Co@C (20 mg), H_2O (5 mL), 140 °C, and 20 bar of H_2. HMF (◆), BHMF (▪), HCPENT (▲), HCPN (×), HCPO (✱), HHD (—).

observed in the $Ni_{0.5}Co_{0.5}$ sample. The high selectivity to HCPN exhibited by this catalyst can be attributed to their higher fraction of surface metal sites and to the formation of NiCo alloy that limits the parallel formation of BHMTHF as by-product as well the subsequent hydrogenation of HPCN into HPCO. Thus, in the NiCo alloy catalyst the intrinsic activity of Ni for hydrogenation of C=C bonds is strongly decreased, while the high catalytic activity of Co for the hydrogenation of the C=O bond of cyclopentanone is reduced. This should be due to the preferential adsorption of the aldehyde group of HMF compared with the ketone group on the hydrogenating active sites of the NiCo alloyed structure, resulting in an improved selectivity to the target product (HCPN). When the amount of Co is increased, as in the case of the $Ni_{0.25}Co_{0.75}$@C sample, although NiCo alloyed species are observed, segregated Co^0 surface species are also present, which are highly active for the reduction of HCPN into HCPO, leading then to a decreased selectivity to HPCN.

To verify the existence of a specific effect in the NiCo alloy, an additional catalyst formed by a physical mixture of 50% Ni@C + 50%Co@C was prepared and tested under the same reaction conditions that above. As can be seen in Table 2 (entry 6, and Figure S7), the initial reaction rate of disappearance of HMF with the physical mixture was twofold that of $Ni_{0.5}Co_{0.5}$@C sample; however, the selectivity to the HCPN was considerably lower (65 vs. 92%).

At this point, we have compared the activity and selectivity of the $Ni_{0.5}Co_{0.5}$@C for the hydrogenative ring-rearrangement of HMF with the non-noble metal catalysts previously reported in literature. In Table S1, it can be seen that the $Ni_{0.5}Co_{0.5}$@C catalyst is among the most selective samples.

An issue to be considered here is the origin of acid sites for the ring-rearrangement. It has been observed that slightly acidic conditions, which can be generated by the water dissociation at elevated temperature (the theoretical pH of water at 100 °C is 6.1), are enough to promote the ring-rearrangement.[18] However, it has also been observed that the presence of moderate to weak Lewis acid sites on the catalyst surface (or additives with weak Lewis acidity) can also contribute to the ring-rearrangement.[19] In our work, the amount of oxidized Ni and Co species that could act as Lewis acid sites on surface on the $Ni_{0.5}Co_{0.5}$ sample is very low, and accordingly we can speculate that the acidic contribution of these oxides on the ring-rearrangement should be negligible. In fact, we checked the acidity of the $Ni_{0.5}Co_{0.5}$ sample in an acid-catalyzed reaction test with low demanding acid strength (i.e., acetalization of cyclohexanone with ethanol). The reaction was performed at 120 °C under 20 bar of N_2, and the results showed that the formation of the diethylketal of cyclohexanone was negligible and similar to that obtained with the control experiment (i.e., without the catalyst). Therefore, we suggest that the protons provided from the water dissociation under our reaction conditions are the acid sites that promote the ring-rearrangement, in good agreement with previously reported results where non-acidic supports are involved.[18,28]

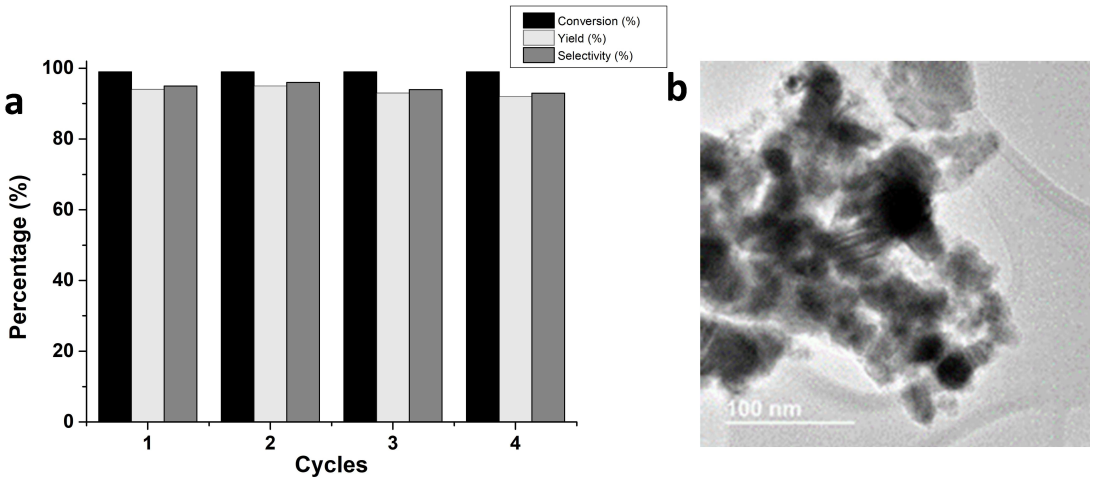

Figure 7. (a) Stability tests of $Ni_{0.5}Co_{0.5}$@C NPs in the hydrogenative ring-rearrangement of HMF. Reaction conditions: HMF (0.5 mmol), 20 mg $Ni_{0.5}Co_{0.5}$@C catalyst, H_2O (5 mL), 140 °C, and 20 bar of H_2 at 7 h reaction time. (b) TEM image of the used $Ni_{0.5}Co_{0.5}$@C catalysts after 4 cycles.

Catalytic stability

Catalytic stability is a very important criterion to evaluate the potential of a catalyst and of particular importance for catalysts that intervene in multistep reactions. Therefore, reusability of the $Ni_{0.5}Co_{0.5}$@C catalyst was studied under 140 °C and 20 bar H_2. For each cycle, the $Ni_{0.5}Co_{0.5}$@C catalyst was easily separated from the reaction with the help of a magnet and reused after pre-activation at 170 °C, 10 bar H_2 during 2 h. As shown in Figure 7a, the $Ni_{0.5}Co_{0.5}$@C catalysts was recycled 4 times, and activity and selectivity to HCPN were preserved through the different runs, indicating the high stability of the catalyst in the hydrogenative ring-rearrangement of HMF. In fact, the TEM image (Figure 7b) and XRD pattern analysis (Figure 8) of the spent catalyst show the unaltered morphological features.

Furthermore, to check if metal leaching occurs during the reaction, an additional experiment was carried out where the reaction was stopped after 1 h. At this point, the catalyst $Ni_{0.5}Co_{0.5}$@C was removed from the hot reaction mixture with a magnet, and the reaction was continued for an additional 6 h. No further HMF conversion was detected during this time (Figure S8), demonstrating that the present catalytic system works in a purely heterogeneous way.

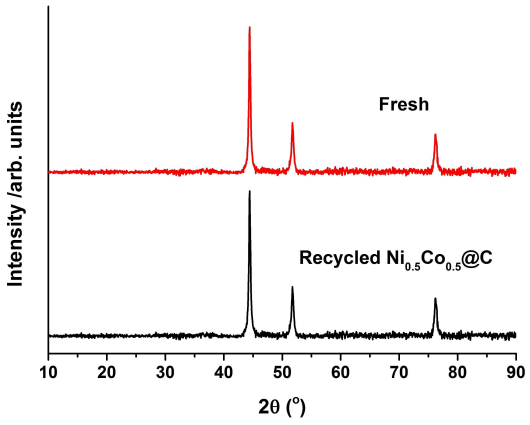

Figure 8. XRD pattern of the fresh and recycled $Ni_{0.5}Co_{0.5}$@C catalysts after 4 cycles.

Synthesis of 3-hydroxymethylcyclopentylamine through a cascade process

Nitrogen-containing compounds, particularly primary amines, are important building blocks widely used to synthesize polymers, agrochemicals, surfactants, and pharmaceuticals.[53,54] Therefore, the sustainable production of nitrogen-containing compounds from renewable biomass derivatives through the reductive amination of carbonyl compounds with ammonia or amines (using molecular hydrogen or other hydrogen sources) has attracted much attention.[16,55] Then, considering the results presented above, we envisaged a one-pot cascade process for the production of 3-hydroxymethylcyclopentylamine, by coupling the hydrogenative ring-rearrangement of HMF into HPCN with the reductive amination of HPCN with ammonia under hydrogen pressure and using the same $Ni_{0.5}Co_{0.5}$@C catalyst.

The cascade process was performed as follows: HMF was converted into HPCN in the presence of $Ni_{0.5}Co_{0.5}$@C catalyst, using hydrogen, water as a solvent, at 140 °C and 20 bar during 7 h, achieving > 90% yield of HCPN. After that, 1.5 mL of NH_3 in solution (25 wt%) was added, and the reactor charged with 20 bar H_2. The mixture was stirred at 140 °C for 8 h. After this time, a total conversion of HCPN with 97% selectivity (total selectivity 91%) of 3-hydroxymethylcyclopentylamine was obtained.

Finally, we have studied the catalyst recyclability for the one-pot process. As shown in Figure 9, $Ni_{0.5}Co_{0.5}$ @C catalyst was reused for six consecutive runs maintaining activity and selectivity. No metal leaching occurred in the reaction medium, as revealed by inductively coupled plasma-mass spectrometry (ICP-MS) analysis of the filtrates. Moreover, XRD analysis of the

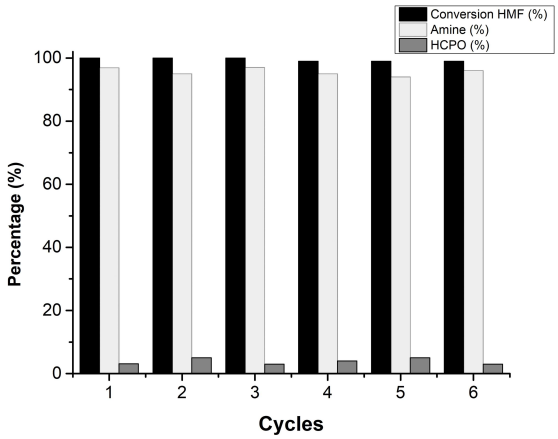

Figure 9. Stability test of $Ni_{0.5}Co_{0.5}$@C catalyst in the one-pot reaction. Reaction conditions: HMF (0.5 mmol), 20 mg $Ni_{0.5}Co_{0.5}$@C catalyst, H_2O (5 mL), NH_3 (1.5 mL, 25% aqueous solution), 140 °C, and 20 bar of H_2.

spent sample showed the absence of additional diffraction peaks associated to oxide species (Figure 10). TEM analysis of the recycled catalyst showed that, as in the fresh catalyst, the spent sample is formed by monodispersed metal NPs covered with thin carbon films (Figure 11). These results confirm the role

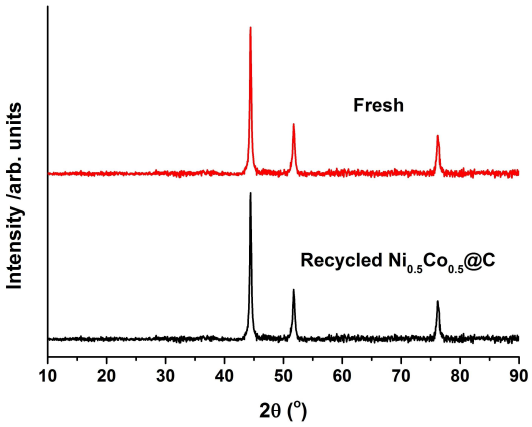

Figure 10. XRD pattern of the fresh and recycled $Ni_{0.5}Co_{0.5}$@C catalysts after 3 cycles in cascade process.

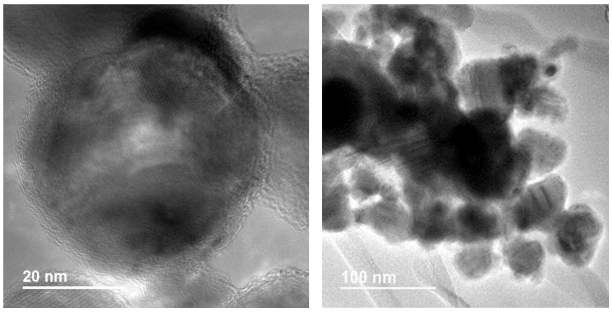

Figure 11. TEM image of the used $Ni_{0.5}Co_{0.5}$@C catalysts after 3 cycles in cascade process.

of the carbon layers on the metal that provides good stability to the NPs, avoiding agglomeration and overoxidation, and allowing a prolonged use.

Conclusions

We have shown that a NiCo alloyed catalyst, with a molar ratio Ni/Co = 1 ($Ni_{0.5}Co_{0.5}$@C), where the metal nanoparticles are partially covered by a thin layer of carbon, exhibits excellent activity and selectivity for performing the hydrogenative ring-rearrangement of 5-hydroxymethylfurfural (HMF) into 3-hydroxymethylcyclopentanone (HCPN). The behavior of the catalyst can be attributed to the formation of NiCo alloy structures that limits competitive reactions such the hydrogenation of furan ring and the over-reduction of the formed HPCN. Compared with other non-noble metal catalysts previously reported for this transformation, the $Ni_{0.5}Co_{0.5}$@C gives high activity and selectivity. Moreover, it is shown for the first time that HMF can be directly converted into the highly valuable 3-hydroxymethylcyclopentylamine through a one-pot cascade process involving hydrogenative ring-rearrangement of HMF into HCPN followed by the reductive amination of HPCN with ammonia on the same $Ni_{0.5}Co_{0.5}$@C catalyst and in the same reaction media. The catalyst shows remarkably high stability, maintaining its activity and selectivity through different consecutive runs, and this can be attributed to the effect of the carbon layers covering and protecting the metal species. Several aspects in terms of sustainability of the process are outstanding: water is used as solvent, aqueous solution of ammonia is used as nitrogen source (rather than pressurized ammonia gas), and the catalytic system works under mild reaction conditions.

Experimental Section

Synthesis of catalysts of Ni@C and Co@C

Co_3O_4 NPs were first prepared following a reported procedure.[32] Typically, 4.94 g of $Co(Ac)_2$ were dissolved in 100 mL of ethylene glycol with stirring at 160 °C, and an aqueous solution of Na_2CO_3 (4.24 g of Na_2CO_3 in 160 mL of distilled water) was added dropwise over approximately 1.5 to 2 h. Next, the suspension was aged for 1 h before cooling. After filtering and washing with water and acetone, a solid purple product was obtained. After drying in an oven at 60 °C for 16 h, the solid was calcined in air at 450 °C for 3 h with a ramp of 1 °C min^{-1} from room temperature to 450 °C. Then, 0.5 g of Co_3O_4 NPs were dispersed in an aqueous glucose solution (360 mg of glucose dissolved in 20 mL distilled water) under ultrasonic treatment. The black suspension was transferred to a 35 mL stainless-steel autoclave equipped with a Teflon liner and kept at 175 °C for 18 h. After cooling down to room temperature, the solid was washed with water and acetone and dried in oven at 60 °C, resulting in two-dimensional $Co(OH)_2$/C composites. Finally, Co@C NPs was obtained by annealing the $Co(OH)_2$/C composites in N_2 at 600 °C for 2 h with a ramp rate of 10 °C min^{-1}. The sample was cooled down in N_2 flow to room temperature and stored in a glass vial. The Ni@C sample was prepared following the same procedure but using 7.0 g of $Ni(Ac)_2 \cdot 4H_2O$ salt.

Synthesis of bimetallic NiCo@C catalysts

Following the same methodology, the bimetallic catalysts NiCo@C with different Ni/Co molar ratios (0.33, 1, and 3) were prepared starting from Ni and Co salts. Typically, for the $Ni_{0.5}Co_{0.5}$@C sample, 3.36 g of $Co(Ac)_2$ and 4.72 g $Ni(Ac)_2 \cdot 4H_2O$ were dissolved in 100 mL of ethylene glycol under stirring at 160 °C and a solution of Na_2CO_3 (5.0 g of Na_2CO_3 in 160 mL of distilled water) was added drop by drop. It took between 1.5 and 2 h to finish the process. The suspension was then aged for 1 h before cooling. After filtering the suspension and washing with water and acetone, the solid obtained was dried in an oven at 60 °C for 16 h and then was calcined in air at 450 °C for 3 h with a ramp of 1 °C min^{-1} from room temperature to 450 °C. Next, the oxides obtained were submitted to the hydrothermal treatment with aqueous solution of glucose, and subsequently annealed at 600 °C following the procedure described above, giving the NiCo@C catalysts. The chemical composition of the different NiCo catalysts was determined by ICP analysis (Table S2).

Catalysts characterization

Powder XRD experiments were carried out with a Philips X'Pert diffractometer equipped with a PW3050 goniometer using CuK_α radiation and a multisampling handler.

Samples for electron microscopy studies were dispersed in CH_2Cl_2 and transferred directly onto holey-carbon coated copper grids. All the measurements were performed using a JEOL JEM2100F microscope operating at 200 kV in both transmission (TEM) and scanning-transmission modes (STEM). STEM images were obtained using a HAADF detector, which allows Z-contrast imaging.

XPS spectra of the catalysts were collected using a SPECS spectrometer equipped with a 150-MCD-9 multichannel analyzer and using non-monochromatic MgK_α (1253.6 eV) irradiation. Spectra were recorded using an analyzer pass energy of 30 eV, an X-ray power of 100 W, and under an operating pressure of 10^{-9} mbar. Peak intensities were calculated after nonlinear Shirley-type background subtraction and corrected by the transmission function of the spectrometer. During data processing of the XPS spectra, BE values were referenced to C 1s peak (284.5 eV). CasaXPS software was used for spectra treatment. The H_2 pretreatment of the samples was performed in a reaction cell connected to XPS analysis chamber and transferred into the XPS analysis chamber without contact with air.

The redox properties of NiCo@C samples were evaluated by TPR. Micromeritics AutoChem 2910 catalyst characterization system with a thermal conductivity detector (TCD) was used. Prior to each experiment, about 40 mg of sample was pretreated at room temperature in flowing He (10 mL min^{-1}) for 20 min. The sample was treated by heating from 25 to 600 °C at a rate of 5 °C min^{-1} in a flow of 10 vol% H_2 in Ar. The total gas flow rate was 50 mL min^{-1}.

Catalytic experiments

Rearrangement of HMF into HCPN: Reactions were carried out in a batch stirred stainless-steel autoclave of 12 mL, equipped with a Teflon vessel, a pressure controller, and a cannula that allowed samples to be taken during the reaction. In a typical experiment, the Teflon vessel containing a stir bar was loaded with 20 mg of catalyst and placed in the stainless-steel autoclave. After sealing, the autoclave was purged three times with H_2, pressurized at 20 bar H_2, and kept at 200 °C for 2 h. Then, the autoclave was cooled to room temperature and depressurized. Without opening the autoclave, a mixture of HMF (0.5 mmol) dissolved into 5 mL of deionized water was added through the cannula. Next, the reactor was pressurized at 20 bar of H_2 and heated at 140 °C under stirring. Mass transfer limitations and internal diffusion resistance were avoided by ensuring small catalytic particle size (<100 μm) and high stirring speed (1000 rpm). To follow the reaction, aliquots (50 μL) were taken for analysis by GC and GC-MS at different reaction times. After completion of the reaction, the autoclave was cooled to room temperature and depressurized for catalyst recycle experiments. Due to the paramagnetic nature of these catalysts, they could easily be recovered with the magnetic stir bar, washed thoroughly with acetone and deionized water, dried under ambient conditions, and used for the subsequent reaction. The product distribution was determined using an Agilent Technologies 7890A gas chromatograph equipped with a flame ionization detector (FID), while product identification was performed by GC-MS using an Agilent 6890N GC System equipped with an HP-5 column and coupled with an Agilent 5973N mass detector. A DB-WAX 15 × 3.2 mm × 0.25 μm film thickness capillary column was employed. Repeated reactions with different samples from the same batch of catalyst delivered a product composition that was reproducible to within ±5%, and mass balance accounted for >98%.

One-pot cascade process: HMF was converted into HPCN in the presence of 20 mg $Ni_{0.5}Co_{0.5}$@C catalyst, using hydrogen and water as a solvent, at 140 °C and 20 bar during 7 h. After that, the reactor was depressurized, 1.5 mL of aqueous ammonium solution (25 wt%) was added, and the reactor was charged with 20 bar H_2. The mixture was heated at 140 °C for 8 h. At certain time intervals, reaction samples were taken and cooled, their residual free ammonia was volatilized, the catalyst was filtered off, and the samples were analyzed by GC and the products identified by GC-MS.

Acknowledgements

This work has been supported by the Spanish government through the "Severo Ochoa Program" (SEV-2016-0683) and the PGC2018-097277-B-100 (MCIU/AEI/FEDER, UE) project. The authors also thank Microscopy Service of UPV for the TEM measurements.

Conflict of Interest

The authors declare no conflict of interest.

Data Availability Statement

The data that support the findings of this study are available from the corresponding author upon reasonable request.

Keywords: 5-hydroxymethylfurfural · biomass · heterogeneous catalysis · hydrogenative ring-rearrangement · reductive amination

[1] A. Corma, S. Iborra, A. Velty, *Chem. Rev.* **2007**, *107*, 2411–2502.
[2] Y. Wan, J. M. Lee, *ACS Catal.* **2021**, *11*, 2524–2560.
[3] P. Prabhu, Y. Wan, J. M. Lee, *Matter* **2020**, *3*, 1162–1177.
[4] R. J. Van Putten, J. C. Van Der Waal, E. De Jong, C. B. Rasrendra, H. J. Heeres, J. G. De Vries, *Chem. Rev.* **2013**, *113*, 1499–1597.

[5] Q. Hou, X. Qi, M. Zhen, H. Qian, Y. Nie, C. Bai, S. Zhang, X. Bai, M. Ju, *Green Chem.* **2021**, *23*, 119–231.
[6] J. Zhao, A. Jayakumar, Z. T. Hu, Y. Yan, Y. Yang, J. M. Lee, *ACS Sustainable Chem. Eng.* **2018**, *6*, 284–291.
[7] J. Zhao, Y. Yan, Z. T. Hu, V. Jose, X. Chen, J. M. Lee, *Catal. Sci. Technol.* **2020**, *10*, 4179–4183.
[8] E. M. Gallego, M. T. Portilla, C. Paris, A. León-Escamilla, M. Boronat, M. Moliner, A. Corma, *Science* **2017**, *355*, 1051–1054.
[9] K. S. Arias, M. J. Climent, A. Corma, S. Iborra, *ACS Sustainable Chem. Eng.* **2016**, *4*, 6152–6159.
[10] A. Garcia-Ortiz, K. S. Arias, M. J. Climent, A. Corma, S. Iborra, *ChemSusChem* **2018**, *11*, 2870–2880.
[11] K. S. Arias, L. Liu, A. Garcia-Ortiz, M. J. Climent, P. Concepción, S. Iborra, A. Corma, *Catal. Sci. Technol.* **2021**, *11*, 3353–3363.
[12] K. S. Arias, J. M. Carceller, M. J. Climent, A. Corma, S. Iborra, *ChemSusChem* **2020**, *13*, 1864–1875.
[13] J. Ohyama, R. Kanao, A. Esaki, A. Satsuma, *Chem. Commun.* **2014**, *50*, 5633–5636.
[14] T. Kitahara, Y. Warita, M. Abe, M. Seya, Y. Takagi, K. Mori, *Agric. Biol. Chem.* **1991**, *55*, 1013–1017.
[15] P. Marcé, Y. Díaz, M. I. Matheu, S. Castillón, *Org. Lett.* **2008**, *10*, 4735–4738.
[16] J. He, L. Chen, S. Liu, K. Song, S. Yang, A. Riisager, *Green Chem.* **2020**, *22*, 6714–6747.
[17] H. Rapoport, Y. Chen, R. M. Mohareb, J. H. Ahn, T. B. Sim, J. Z. Ho, *Chem. Pharm. Bull.* **2003**, *51*, 1153–1156.
[18] S. Zhang, H. Ma, Y. Sun, Y. Luo, X. Liu, M. Zhang, J. Gao, J. Xu, *Green Chem.* **2019**, *21*, 1702–1709.
[19] J. Ohyama, Y. Ohira, A. Satsuma, *Catal. Sci. Technol.* **2017**, *7*, 2947–2953.
[20] S. Sitthisa, D. E. Resasco, *Catal. Lett.* **2011**, *141*, 784–791.
[21] Q. Deng, R. Gao, X. Li, J. Wang, Z. Zeng, J. J. Zou, S. Deng, *ACS Catal.* **2020**, *10*, 7355–7366.
[22] X. Li, Q. Deng, S. Zhou, J. Zou, J. Wang, R. Wang, Z. Zeng, S. Deng, *J. Catal.* **2019**, *378*, 201–208.
[23] Q. Deng, X. Wen, P. Zhang, *Catal. Commun.* **2019**, *126*, 5–9.
[24] X. Li, Q. Deng, L. Zhang, J. Wang, R. Wang, Z. Zeng, S. Deng, *Appl. Catal. A* **2019**, *575*, 152–158.
[25] M. Le Besson, P. Gallezot, C. Pinel, *Chem. Rev.* **2013**, *114*, 1827–1870.
[26] N. Perret, A. Grigoropoulos, M. Zanella, T. D. Manning, J. B. Claridge, M. J. Rosseinsky, *ChemSusChem* **2016**, *9*, 521–531.
[27] R. Ramos, A. Grigoropoulos, N. Perret, M. Zanella, A. P. Katsoulidis, T. D. Manning, J. B. Claridge, M. J. Rosseinsky, *Green Chem.* **2017**, *19*, 1701–1713.
[28] M. V. Morales, J. M. Conesa, A. Guerrero-Ruiz, I. Rodríguez-Ramos, *Carbon N Y* **2021**, *182*, 265–275.
[29] S. K. Singh, *Asian J. Org. Chem.* **2018**, *7*, 1901–1923.
[30] J. Li, Y. Feng, H. Wang, X. Tang, Y. Sun, X. Zeng, L. Lin, *J. Mol. Catal.* **2021**, *505*, 111505–111512.
[31] M. Puche, L. Liu, P. Concepción, I. Sorribes, A. Corma, *ACS Catal.* **2021**, *11*, 8197–8210.
[32] L. Liu, F. Gao, P. Concepción, A. Corma, *J. Catal.* **2017**, *350*, 218–225.
[33] L. Liu, P. Concepción, A. Corma, *J. Catal.* **2016**, *340*, 1–9.
[34] L. Liu, P. Concepción, A. Corma, *J. Catal.* **2019**, *369*, 312–323.
[35] W. Peng, J. Jin, S. Yang, Z. Shen, H. Wang, J. Zhang, G. Li, *ACS Appl. Energ. Mater.* **2021**, *4*, 11041–11050.
[36] X. He, F. Yin, G. Li, B. Chen, S. Wang, M. Gu, *J. Mater. Chem. A.* **2020**, *8*, 25805–25823.
[37] S. Yao, X. Wang, Y. Jiang, F. Wu, X. Chen, X. Mu, *ACS Sustainable Chem. Eng.* **2014**, *2*, 173–180.
[38] J. Long, K. Shen, L. Chen, Y. Li, *J. Mater. Chem. A.* **2016**, *4*, 10254–10262.
[39] X. Zhang, J. Wang, Y. Fan, H. Ren, Z. Liu, Y. Wang, Y. Liu, H. Bai, L. Kong, *Nanotechnology* **2021**, *32*, 385602.
[40] Y. Shi, L. Ai, H. Shi, X. Gu, Y. Han, J. Chen, *Front. Chem.* **2021**, *1*, 156–163.
[41] D. Wang, W. Gong, J. Zhang, M. Han, C. Chen, Y. Zhang, G. Wang, H. Zhang, H. Zhao, *Chin. J. Catal.* **2021**, *42*, 2027–2037.
[42] A. R. Denton, N. W. Ashcroft, *Phys. Rev. A* **1991**, *43*, 3161–3164.
[43] G. Qian, J. Chen, T. Yu, L. Luo, S. Yin, *Nano-Micro Lett.* **2021**, *13*, 77.
[44] H. Wang, X. Li, X. Lan, T. Wang, *ACS Catal.* **2018**, *8*, 2121–2128.
[45] Y. T. Law, T. Dintzer, S. Zafeiratos, *Appl. Surf. Sci.* **2011**, *258*, 1480–1487.
[46] M. C. Biesinger, B. P. Payne, A. P. Grosvenor, L. W. M. Lau, A. R. Gerson, R. S. C. Smart, *Appl. Surf. Sci.* **2011**, *257*, 2717–2730.
[47] G. Moretti, *The Auger parameter, in Surf. Anal. by Auger X-Ray Photoelectron Spectrosc.* (Eds.: D. Briggs, J. T. Grant), IM Publications, Chichester, **2003**, pp. 501–530.
[48] C. D. Wagner, A. V. Naumkin, A. Kraut-Vass, J. W. Allison, C. J. Powell, J. R. Rumble Jr., "NIST X-ray Photoelectron Spectroscopy (XPS) Database, Version 3.4," https://srdata.nist.gov/xps/, **2003**.
[49] X. Kong, Y. Zhu, H. Zheng, F. Dong, Y. Zhu, Y.-W. Li, *RSC Adv.* **2014**, *4*, 60467–60472.
[50] C. Zeng, H. Seino, J. Ren, K. Hatanaka, N. Yoshie, *Polymer* **2013**, *54*, 5351–5357.
[51] X.-L. Li, J. Deng, J. Shi, T. Pan, C.-G. Yu, H.-J. Xu, Y. Fu, *Green Chem.* **2015**, *17*, 1038–1046.
[52] R. Ramos, A. Grigoropoulos, N. Perret, M. Zanella, A. P. Katsoulidis, T. D. Manning, J. B. Claridge, M. J. Rosseinsky, *Green Chem.* **2017**, *19*, 1701–1713.
[53] D. Talwar, P. Salguero, C. M. Robertson, J. Xiao, *Chem. Eur. J.* **2014**, *20*, 245–252.
[54] J. Gallardo-Donaire, M. Ernst, O. Tr, T. Schaub, *Adv. Synth. Catal.* **2016**, *358*, 358–363.
[55] M. Pelckmans, T. Renders, S. Van De Vyver, B. F. Sels, *Green Chem.* **2017**, *19*, 5303–5331.

Manuscript received: January 27, 2022
Revised manuscript received: March 31, 2022
Accepted manuscript online: April 1, 2022
Version of record online: May 12, 2022